Magnetization and specific heat of $TbFe_3(BO_3)_4$: Experiment and crystal-field calculations

E. A. Popova, D. V. Volkov, and A. N. Vasiliev
Low Temperature Physics Department, Physics Faculty, Moscow State University, 119992 Moscow, Russia

A. A. Demidov and N. P. Kolmakova*
Bryansk State Technical University, 241035 Bryansk, Russia

I. A. Gudim and L. N. Bezmaternykh
L.V. Kirensky Institute of Physics, Siberian Branch of RAS, 660036 Krasnoyarsk, Russia

N. Tristan,† Yu. Skourski, B. Büchner, C. Hess, and R. Klingeler
Leibniz-Institute for Solid State and Materials Research, IFW Dresden, 01171 Dresden, Germany
(Received 19 April 2006; revised manuscript received 27 October 2006; published 13 June 2007)

We have studied the thermodynamic properties of single-crystalline $TbFe_3(BO_3)_4$. Magnetization measurements have been carried out as a function of magnetic field (up to 50 T) and temperature up to 350 K with the magnetic field both parallel and perpendicular to the trigonal c axis of the crystal. The specific heat has been measured in the temperature range 2–300 K with a magnetic field up to 9 T applied parallel to the c axis. The data indicate a structural phase transition at 192 K and antiferromagnetic spin ordering at $T_N \approx 40$ K. A Schottky anomaly is present in the specific-heat data around 20 K, arising due to two low-lying energy levels of the Tb^{3+} ions being split by f-d coupling. Below T_N, magnetic fields parallel to the c axis drive a spin-flop phase transition, which is associated with a large magnetization jump. The highly anisotropic character of the magnetic susceptibility is ascribed mainly to the Ising-like behavior of the Tb^{3+} ions in the trigonal crystal field. We describe our results in the framework of a unified approach which is based on mean-field approximation and crystal-field calculations.

DOI: 10.1103/PhysRevB.75.224413 PACS number(s): 75.30.−m, 75.40.Cx, 71.70.−d

I. INTRODUCTION

The family of ferroborates with the general formula $RFe_3(BO_3)_4$ (R is a rare-earth ion or Y) attracts considerable attention since its members exhibit a wide variety of phase transitions. They possess magnetic structures which change as a function of temperature, external magnetic field, and substitutions in the rare-earth subsystem.[1–4] It was recently discovered that $RFe_3(BO_3)_4$ (R=Gd,Nd) exhibits multiferroic features, i.e., the coexistence of elastic, magnetic, and electric order parameters.[5–7] The various ordering phenomena and their interaction cause anomalies in the dielectric permeability, electric polarization, and magnetostriction, both spontaneous and field induced. Our study aims to elucidate this interplay for the ferroborate $TbFe_3(BO_3)_4$, in which both the rare-earth ions and the Fe ions form a magnetic subsystem.

The crystal structure of $TbFe_3(BO_3)_4$ at high temperatures is trigonal and belongs to the space group D_3^7 ($R32$).[1,8,9] The main elements of the structure are spiral chains of edge-sharing FeO_6 octahedra running along the c axis. The rare-earth ions are coordinated by triangular RO_6 prisms which are isolated from each other since they are separated by regular BO_3 triangles and have no common oxygen ions. Both the BO_3 triangles and RO_6 prisms connect three FeO_6 chains. There are no direct Fe-O-Fe links within the same c plane and the shortest interchain exchange paths are therefore given by Fe-O-R-O-Fe and Fe-O-B-O-Fe, while the Fe-O-Fe exchange paths within the chains are much shorter (see Fig. 1). In the case of $GdFe_3(BO_3)_4$, the room-temperature struc-

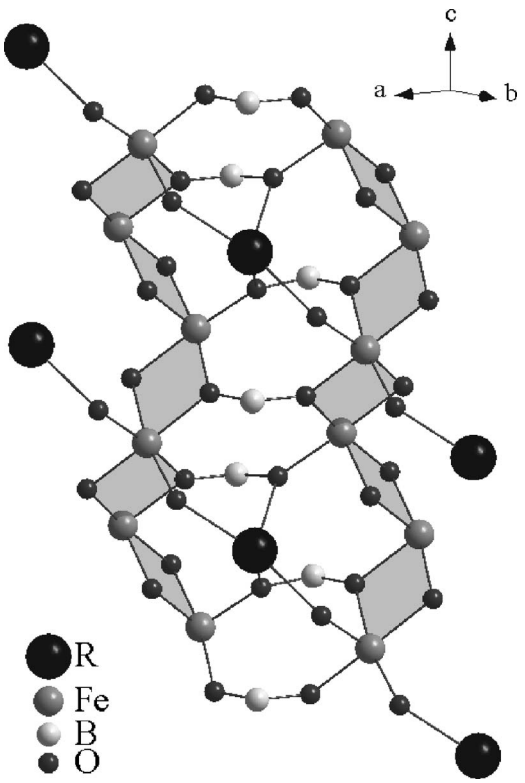

FIG. 1. The crystal structure of $RFe_3(BO_3)_4$. The spiral chains formed by FeO_6 octahedra along the c axis (the shortest Fe-O-Fe exchange) are represented by the chains of shadowed areas.

ture was found to be transformed to the D_3^4 ($P3_121$) space group at T_S=156 K.[4,9] Below T_S, two nonequivalent Fe sites are present, which give rise to both a stretched and a compressed modification of the FeO_6 spiral chains.

In $GdFe_3(BO_3)_4$, the presence of different magnetic sublattices causes several magnetic transitions below T_S, which are associated with antiferromagnetic spin ordering of the Fe sublattice ($T_N \approx 37$ K) and a spin reorientation at $T_{SR} \approx 9$ K.[4,10–12] In addition, strong magnetostrictive and magnetoelectric effects below T_{SR} are associated with a spin reorientation which occurs in external magnetic fields with $B \| c$ axis.[5–7]

In this paper, we report on the thermodynamic properties of $TbFe_3(BO_3)_4$. Our data on $TbFe_3(BO_3)_4$ show a spin-flop phase transition, which is driven by magnetic fields $B \| c$. This transition is associated with a large jump of the magnetization. The highly anisotropic magnetic susceptibility is ascribed mainly to the Ising-like behavior of the Tb^{3+} ions in the trigonal crystal field. Our experimental data are analyzed in the context of the unified approach which is based on mean-field approximation and crystal-field calculations. The spin-flop transition is apparently accompanied by magnetoelastic effects. Magnetoelectric effects might therefore be associated with the spin-flop transition, leading $TbFe_3(BO_3)_4$ to be a candidate for a multiferroic compound.

II. EXPERIMENT

The single crystals of $TbFe_3(BO_3)_4$ were grown using a $Bi_2Mo_3O_{12}$-based flux.[13] The seeds were obtained by spontaneous nucleation from the same flux. Single crystals were green in color and had a good optical quality. The orientation of the crystals was performed by x-ray diffraction. All magnetic measurements were performed with the external magnetic field either parallel or perpendicular to the c axis of the crystal. The ac susceptibility at 1000 Hz and the dc susceptibility were measured in magnetic fields of 0.001 and 0.1 T, respectively, in the temperature range 1.8–350 K using a Quantum Design physical property measurement system (PPMS). The magnetization $M(B)$ was measured between 4.2 and 120 K in fields up to 15 T with a vibrating sample magnetometer (VSM).[14] The field sweep rate was approximately 0.2 T/min. In addition to this, a pulsed field magnetometer was used for magnetization measurements up to 50 T.[15] Here, the total pulse duration amounted to 0.05 s. The temperature dependence of the specific heat was measured in the temperature range 1.8–300 K and in magnetic fields up to 9 T with a PPMS calorimeter.

III. EXPERIMENTAL RESULTS

$TbFe_3(BO_3)_4$ exhibits two phase transitions below room temperature, as is illustrated by the specific-heat and magnetization data in Fig. 2. By comparison with $GdFe_3(BO_3)_4$, the first-order phase transition at T_S=192 K is tentatively attributed to a structural symmetry reduction to the low symmetric $P3_121$ phase.[9] Actually, the data exhibit several first-order anomalies of the specific heat in the vicinity of T_S, which are probably related to structural changes. The origin of these

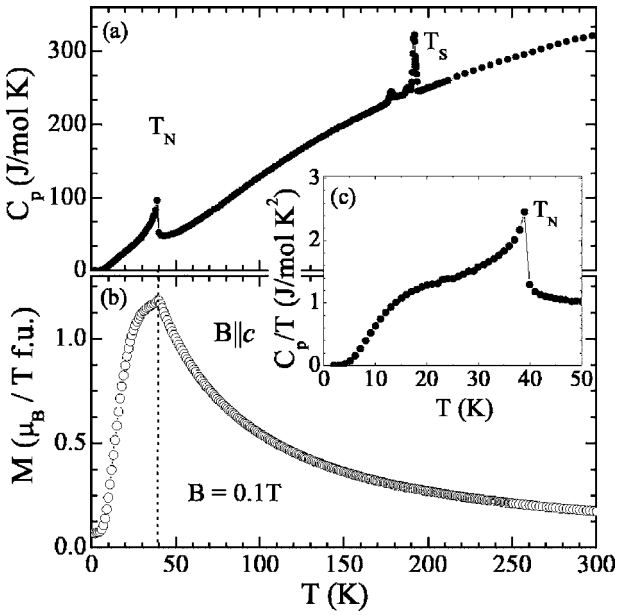

FIG. 2. Specific heat in (a) zero magnetic field and (b) magnetization at B=0.1 T of $TbFe_3(BO_3)_4$. Inset (c) highlights the Schottky anomaly of C_p/T at $T \sim 20$ K. T_S and T_N label the (presumably) structural phase transition and the onset of antiferromagnetic spin ordering in the Fe sublattice, respectively.

anomalies cannot be clarified by our present study which focuses on the magnetic properties of $TbFe_3(BO_3)_4$. The structural phase transition is associated with an entropy jump of $\Delta S \approx 1.9$ J/mol K. At T_N=40 K, the onset of antiferromagnetic spin order in the iron subsystem is demonstrated by a sharp jump in the specific heat and a kink in the magnetization. We observe a specific-heat jump of $\Delta C_p \approx 59.4$ J/mol K. This result agrees with the jump ΔC_p which is predicted from the mean-field theory for the antiferromagnetic spin ordering of the S=5/2 Fe sublattice:[16]

$$\Delta C_p = \frac{5S(S+1)}{S^2 + (S+1)^2} R = 59 \text{ J/mol K}, \quad (1)$$

with R being the gas constant. The entire spin entropy of the Fe^{3+} subsystem appears to develop only below T_N. The Fe^{3+} subsystem must therefore be considered as a classical three-dimensional (3D) antiferromagnet, since short-range spin correlations at significantly higher temperatures, which would be present if the Fe^{3+} chains were able to form quasi-one-dimensional magnets, are clearly absent. An analysis of the specific-heat data[10] indeed confirms that the magnetic ordering only occurs in the Fe subsystem, while the Tb subsystem is polarized by the Fe subsystem.

In contrast to the anomalies due to the structural and magnetic phase transitions at T_S and T_N, respectively, the Schottky anomaly in the specific heat at ~20 K reveals the temperature-driven population of the ground state of the Tb^{3+} ion split in the magnetic field of the Fe subsystem. No spin reorientation [similar to the one seen in $GdFe_3(BO_3)_4$ ferroborate] was observed at low temperatures in zero magnetic field.

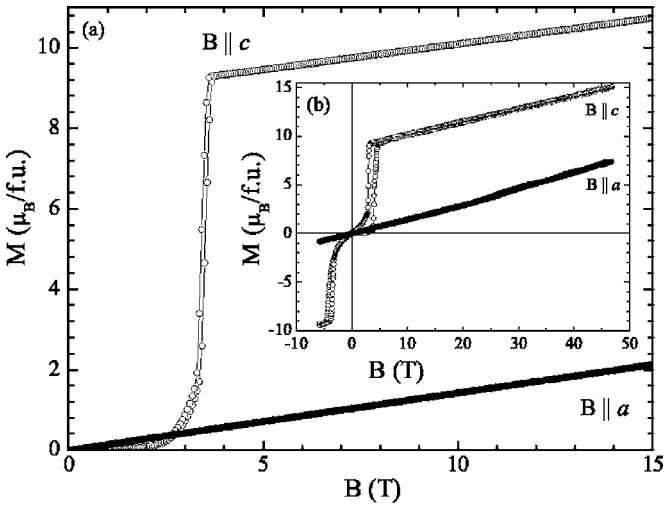

FIG. 3. Magnetization, at $T=4.2$ K, for the magnetic field applied to the c and a axes. Data obtained in a quasistatic field (VSM) are shown in (a), whereas (b) displays pulsed magnetic field data (see text).

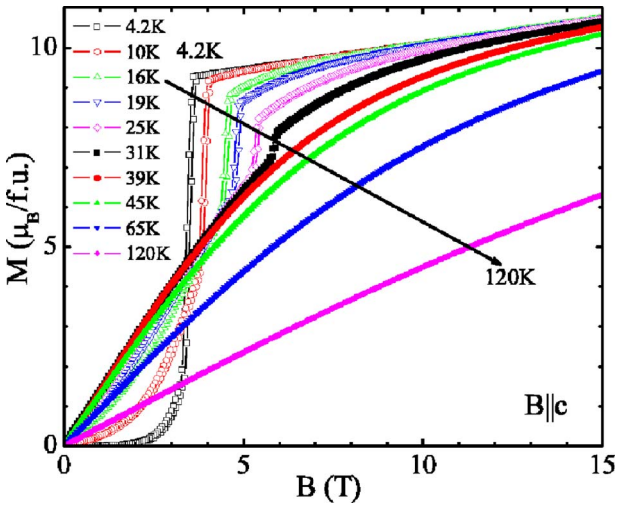

FIG. 4. (Color online) Magnetization for the magnetic field applied to the c axis at various fixed temperatures.

Depending on their direction, external magnetic fields can have a drastic effect on the magnetic properties of $TbFe_3(BO_3)_4$. As shown in Fig. 3, for applied magnetic fields parallel to the a axis there is a linear field dependence of the magnetization at 4.2 K. The data imply $\chi_a=0.14\mu_B$/T f.u. In contrast, applying a magnetic field along the easy magnetic axis, i.e., the trigonal c axis, causes a sharp jump in the magnetization at $B_c(4.2\ \mathrm{K})\sim 3.5$ T. Here, the magnetic field drives a first-order transition. We demonstrate further below that the main feature of this transition is a spin flop of the anti-ferromagnetically ordered Fe^{3+} spins which is accompanied by the orientation of magnetic moments of the Tb^{3+} subsystem along the external magnetic field. The strongly discontinuous character of the transition is illustrated also by the pulsed field data in Fig. 3(b). In the pulsed field ($\partial B/\partial t\sim 5000$ T/s), the hysteresis at the spin-flop transition is 1 order of magnitude larger than in the quasistatic measurement ($\partial B/\partial t\sim 10^{-3}$ T/s) shown in Fig. 3(a), due to the relaxation processes and magnetocaloric effect. At high magnetic fields $B>B_c$, the data show a linear $M(B)$ curve with $\chi_c=0.13\mu_B$/T f.u. being slightly smaller than χ_a.

The magnetization data in Fig. 3 show a strong anisotropy. It is reasonable (and will be shown in Sec. V in a detailed analysis) to attribute this anisotropy to the highly anisotropic Tb^{3+} magnetic moments, which are subject to the staggered field of the antiferromagnetically ordered Fe spins. The discussion hence must not only address the two subsystems of Fe and Tb moments, of which the Fe system divides in the two sublattices below T_N, but also discuss the Tb subsystem in terms of two sublattices since it is polarized by the indirect exchange interaction with the iron subsystem.

The field dependence of the magnetization at 4.2 K shown in Fig. 3 reveals two anisotropy features: (1) A sharp increase of the magnetic moment $\sim 9\mu_B$ evolves at the critical field B_c. (2) The linear contribution to $M(B\|c)$ only exists above B_c. If the extra moment (1) is neglected, the linear part of $M(B\|c)$ is a straight line through the origin which is very similar to $M(B\|a)$. Such behavior (2) is typical for a uniaxial antiferromagnet magnetized along the easy axis.

Upon heating (see Fig. 4), the spin-flop transition shifts to higher temperatures and vanishes above T_N, but it remains clearly visible in the entire antiferromagnetically spin ordered phase. However, the magnetization jump reduces in value and becomes less sharp as it is shifted toward higher fields. For fields larger than B_c as well as for $T>T_N$, the magnetization curves become nonlinear.

Below T_N and for fields $B\|c<B_c$, the staggered field of the Fe spins polarizes the terbium subsystem due to f-d interactions, yielding two Tb sublattices with the magnetic moments oriented oppositely and along the c axis. For $B\|c$, the effective field acting on the terbium sublattice which magnetic moment opposes the applied field is decreased as the applied field increases and this magnetic moment tends to diminish. This is a factor determining the character of the magnetization at 4.2 K prior to the phase transition, since at low temperatures the longitudinal susceptibility of the iron subsystem is very small. At B_c, the staggered field acting on the Tb^{3+} magnetic moments vanishes as the magnetic moments of Fe^{3+} ions become oriented nearly perpendicular to them. As a result, the magnetic moments of Tb^{3+} ions align with the external magnetic field, reaching the saturation value of about $9\mu_B$ at low temperatures.

In the spin-flop phase, both terbium sublattices have magnetic moments directed along the field $B\|c$ and the magnetic moments of iron sublattices bend toward the field direction. This part of the magnetization curve allows us to estimate the transverse susceptibility of the iron subsystem: $\chi_\perp^{\mathrm{Fe}}\approx\chi_c=0.13\mu_B$/T f.u. The observation of $\chi_a>\chi_c$ suggests a small contribution from the Tb subsystem for $B\|a$. At higher temperatures, as shown in Fig. 4, the magnetization curves gradually become less sharp. In the initial collinear phase, the iron subsystem begins to contribute to the magnetization as longitudinal susceptibility grows with increasing temperature, thus stabilizing the initial phase.

The magnetic phase diagram, constructed from these data and from specific-heat measurements in magnetic fields, is

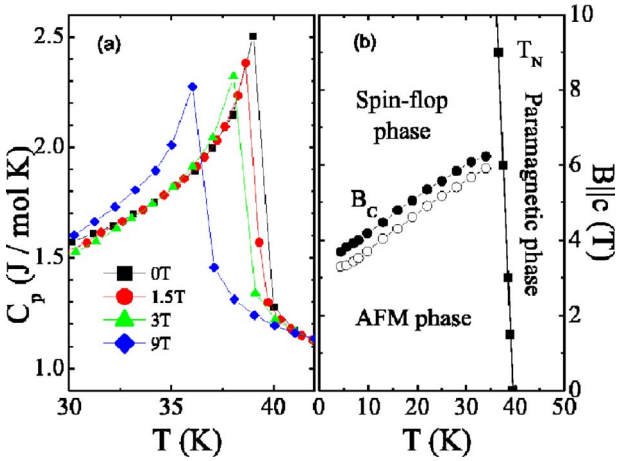

FIG. 5. (Color online) (a) Specific-heat anomaly at T_N for different magnetic fields and (b) magnetic phase diagram for $B \| c$ from magnetization and specific-heat data. B_c labels the critical field of the spin-flop transition. Full (open) data markers refer to increasing (decreasing) quasistatic fields, i.e., $\partial B/\partial t \sim 10^{-3}$ T/s (see the text).

presented in Fig. 5. The difference in phase boundaries shown by open and full symbols accounts for the hysteretic phenomena and finite slope of $M(B)$ curves at the spin-flop transition. This diagram shows that magnetic fields parallel to the c axis slightly suppress the antiferromagnetic spin ordering temperature of the Fe sublattice. In contrast, the critical field of the spin-flop transition increases upon heating.

IV. THEORY

The magnetic properties of terbium ferroborate are governed by both magnetic subsystems interacting with each other. As already mentioned above, the crystal structure of rare-earth ferroborates[1,2,8,9] suggests that the main feature of their magnetic structure is formed by the helical iron chains along the c axis. However, our experimental data provide no evidence for quasi-one-dimensional magnetic properties, which indicates significant interactions between the chains. Moreover, the experimental magnetization curves and phase diagram have the form which is typical for 3D uniaxial antiferromagnets. This fact provides reason enough to consider the magnetic structure of the Fe subsystem as that of uniaxial antiferromagnet with two sublattices, magnetic moments of which are equal in the absence of field. The interaction hierarchy in the system is such that it stabilizes the orientations of Fe and Tb magnetic moments along the trigonal axis. Indeed, the strongest interaction in the compound is the crystal field (the splitting of the ground multiplet comprises about 400–500 cm^{-1}, the energy interval between the ground quasidoublet and the nearest excited states is of the order of 200 cm^{-1}), and the non-Kramers Tb^{3+} ion in the trigonal crystal field acquires a huge anisotropy ($g_c \sim 18, g_a \sim 0$) and becomes an Ising ion with the preferred orientation of magnetic moment along the trigonal axis. Interaction comparable in value with the crystal field is absent in the system; therefore, there is no source of any other orientation of Tb magnetic moments. So there are grounds to suggest a collinear arrangement of magnetic moments in $TbFe_3(BO_3)_4$. We note, however, that only neutron-diffraction studies on an 11B-enriched compound can unambiguously resolve the magnetic structure under discussion.

In the following section, we model the magnetic properties of $TbFe_3(BO_3)_4$ using molecular-field theory. Within this approximation, the total Hamiltonian, which comprises the Hamiltonians of the iron and the terbium subsystems as well as the one considering the Tb-Fe interaction, can be expressed as a sum of single-particle Hamiltonians. In the presence of an external magnetic field B, the effective Hamiltonians of the Tb and Fe ions of the ith sublattice ($i=1$ and 2) can be written as

$$\mathcal{H}_i(\mathrm{Tb}) = \mathcal{H}^i_{CF} - g_J \mu_B \mathbf{J}_i [\mathbf{B} + \mathbf{B}_{mi}(\mathrm{Tb})], \tag{2}$$

$$\mathcal{H}_i(\mathrm{Fe}) = - g_S \mu_B \mathbf{S}_i [\mathbf{B} + \mathbf{B}_{mi}(\mathrm{Fe})], \tag{3}$$

where g_J is the Lande factor and $\mathbf{J}_i$ is the angular momentum operator of the rare-earth ion; $g_S=2$ is the g factor and $\mathbf{S}_i$ is the spin momentum operator of the Fe ion; $\mathbf{B}_{mi}$(Tb/Fe) are the molecular fields acting on the Tb or Fe ion in the ith sublattice. The crystal-field Hamiltonian $\mathcal{H}_{CF}$ is governed by the symmetry of the local environment of the rare-earth ion.

As explained in Sec. III, from the analogy to the structural phase transition at 156 K in $GdFe_3(BO_3)_4$, we suppose that the specific-heat anomaly at $T_S=192$ K reflects a crystal symmetry reduction from the trigonal space group $R32$ to the trigonal group $P3_121$. This implies that the local symmetry of the Tb^{3+} ion is reduced from D_3 at $T > T_S$ to C_2 at $T < T_S$. Nevertheless (as will be discussed below), a simpler Hamiltonian of D_3 symmetry is sufficient for describing the low-temperature magnetic properties of $TbFe_3(BO_3)_4$, since the available crystal-field parameters of isostructural compounds give rise to two closely spaced (with a splitting less than 2–3 cm^{-1}) singlets as a low-lying state of the ground multiplet. These singlets are responsible for the Ising-like behavior of this non-Kramers ion in both the paramagnetic and the ordered phases.

In order to describe the thermodynamic properties of rare-earth compounds, we only need to consider the ground multiplet. In terms of the equivalent operators O^m_n, the crystal-field Hamiltonian $\mathcal{H}_{CF}$ reads as follows:

$$\mathcal{H}_{CF} = \alpha_J B^0_2 O^0_2 + \beta_J (B^0_4 O^0_4 + B^3_4 O^3_4) + \gamma_J (B^0_6 O^0_6 + B^3_6 O^3_6 + B^6_6 O^6_6), \tag{4}$$

where B^m_n are the crystal-field parameters for the D_3 symmetry, and α_J, β_J, and γ_J are the Stevens coefficients. The former are unknown for the Tb^{3+} ion in $TbFe_3(BO_3)_4$. However, our results depend only weakly on the actual crystal-field parameters since the magnetic properties of $TbFe_3(BO_3)_4$ are essentially controlled by the magnetic behavior of the iron subsystem and by the Ising character of the non-Kramers Tb^{3+} ion in the crystal field of the trigonal symmetry. We hence could not determine the crystal-field parameters from the experimental data. Instead, we have used the crystal-field parameters of the isostructural compounds, in particular, the rare-earth aluminoborates (see, e.g., Ref. 17),

and refined these using the data for crystal-field splitting of Nd^{3+} in $NdFe_3(BO_3)_4$.[18]

We have written the expressions for the molecular fields acting on the Tb and Fe ions from the ith sublattice on the basis of the interaction hierarchy and magnetic structure of $TbFe_3(BO_3)_4$. A detailed analysis of the interactions which was performed for the low-temperature phase of $GdFe_3(BO_3)_4$ in Ref. 12 also seems to be quite applicable to $TbFe_3(BO_3)_4$. According to this analysis, a rare-earth ion does not interact with iron ions from the same c plane but interacts antiferromagnetically with iron ions from the neighboring planes [it is clearly shown in Fig. 7(b) of Ref. 12]. The interaction between rare-earth ions can be neglected because the distances between them are larger than 6 Å and no reasonably superexchange path could be introduced. Consequently, none of the ferroborates demonstrates an intrinsic ordering in the rare-earth subsystem. The molecular fields $\mathbf{B}_{mi}$(Tb) and $\mathbf{B}_{mi}$(Fe) can therefore be written as

$$\mathbf{B}_{mi}(\mathrm{Tb}) = \lambda_{fd}\mathbf{M}_i, \tag{5}$$

$$\mathbf{B}_{mi}(\mathrm{Fe}) = \lambda\mathbf{M}_j + \lambda_{fd}\mathbf{m}_i, \quad j = 1 \text{ or } 2, \quad j \neq i, \tag{6}$$

where $\lambda_{fd} < 0$ and $\lambda < 0$ are the molecular constants of the Tb-Fe and Fe-Fe antiferromagnetic interactions. The magnetic moments $\mathbf{M}_i$ and $\mathbf{m}_i$ of the ith iron and terbium sublattices are defined as

$$\mathbf{M}_i = 3g_S\mu_B\langle\mathbf{S}_i\rangle \quad \text{and} \quad \mathbf{m}_i = g_J\mu_B\langle\mathbf{J}_i\rangle. \tag{7}$$

The thermodynamic potential of the system (per formula unit) has the following form:

$$\Phi(T,B) = \frac{1}{2}\left[-k_BT\sum_{i=1}^{2} \ln Z_i(\mathrm{Tb}) + \frac{1}{2}\sum_{i=1}^{2} g_J\mu_B\langle\mathbf{J}_i\rangle\mathbf{B}_{mi}(\mathrm{Tb}) - 3k_BT\sum_{i=1}^{2} \ln Z_i(\mathrm{Fe}) + \frac{1}{2}\sum_{i=1}^{2} 3g_S\mu_B\langle\mathbf{S}_i\rangle\mathbf{B}_{mi}(\mathrm{Fe})\right], \tag{8}$$

with the partition functions

$$Z_i(\mathrm{Tb/Fe}) = \sum_n \exp\left[\frac{-E_{ni}(\mathrm{Tb/Fe})}{k_BT}\right], \tag{9}$$

where E_{ni}(Tb/Fe) are the eigenvalues of corresponding Hamiltonians [Eqs. (2) and (3)]. To find the magnetic moments of the Tb and Fe subsystems [Eqs. (7)] in the mean-field approximation, one has to solve the self-consistent problem of deducing their values and orientations on the basis of Hamiltonians in Eqs. (2) and (3) while considering the condition of the minimum of the thermodynamic potential [Eq. (8)] for a given temperature and field. The right part of equation for M_i is the relevant Brillouin function, as it should be in the case of an equidistant spectrum which is typical for the Fe^{3+} ion with an orbital singlet as a ground state (S ion). Substituting the magnetic moments for particular phases into the thermodynamic potential [Eq. (8)], we obtain the energies of the phases and find the critical fields for the phase transitions from the condition of their equality. The magnetization of the compound (per f.u.) is given by

$$\mathbf{M} = \frac{1}{2}\sum_{i=1}^{2}(\mathbf{M}_i + \mathbf{m}_i). \tag{10}$$

Both magnetic subsystems contribute to the initial magnetic susceptibility of terbium ferroborate:

$$\chi_i = \chi_i^{\mathrm{Fe}} + \chi_i^{\mathrm{Tb}}, \quad i = \parallel \text{ or } \perp. \tag{11}$$

In the paramagnetic range, where the interaction between iron and terbium subsystems can be neglected, the magnetic susceptibility of the Tb subsystem can be calculated with the help of the well-known Van Vleck formula on the basis of the crystal-field Hamiltonian [Eq. (4)]. For the ordered phase at $T < T_N$ as well as for the paramagnetic phase, the initial magnetic susceptibilities of the compound can easily be found from the initial linear parts of the magnetization curve $M(B)$ calculated for the field along and perpendicular to the trigonal axis.

The contribution of the Tb^{3+} subsystem to the heat capacity of the $TbFe_3(BO_3)_4$ compound can be calculated with the help of the usual expression (per rare-earth ion, i.e., per f.u.)

$$C_{\mathrm{Tb}} = k_B\frac{\langle E^2\rangle - \langle E\rangle^2}{(k_BT)^2}. \tag{12}$$

The thermal averages were calculated for the spectrum of Tb^{3+} ion formed by the crystal field and by interactions with the iron subsystem and an external magnetic field.

V. COMPARISON OF EXPERIMENTAL DATA AND THEORETICAL CALCULATIONS

A. Magnetization

In order to carry out a quantitative analysis of the magnetization curves for $TbFe_3(BO_3)_4$ in accordance with the approach presented in the previous section, the magnetizations in the collinear and flop phases were calculated in the mean-field approximation and the critical fields of the phase transitions B_c were found from the equality of their thermodynamic potentials. In Fig. 6, the experimental and calculated magnetization curves are displayed for several temperatures.

The analysis of the magnetization curve at 4.2 K provides a possibility to determine some parameters of the compound. The f-d interaction parameter $\lambda_{fd} = -0.253$ T/μ_B was calculated by fitting the initial part of $M(B)$ where the contribution of Fe subsystem is negligibly small because of its small longitudinal susceptibility at low temperatures. This value of λ_{fd} is in good accordance with the experimental data for the low-temperature splitting Δ of low-lying singlets of the Tb^{3+} ion in $TbFe_3(BO_3)_4$, which is around 32 cm^{-1}.[19] Reasonable crystal-field parameters for Tb^{3+} in $TbFe_3(BO_3)_4$ yield the g-tensor component along the trigonal axis in the range from 17.5 to 17.8, resulting in a value of $\Delta(T=0\ \mathrm{K}) = \mu_B g_z B_{fd}(T=0\ \mathrm{K}) = \mu_B g_z|\lambda_{fd}|M(T=0\ \mathrm{K}) \approx 31\ \mathrm{cm}^{-1}$.

The value of the exchange Fe-Fe parameter, responsible for the transverse susceptibility, $\lambda_1 = -3$ T/μ_B, has been obtained from the slope of the $M(B)$ dependence measured at $T=4.2$ K in the flop phase. However, if the exchange parameter for the collinear phase is taken equal to this value, then

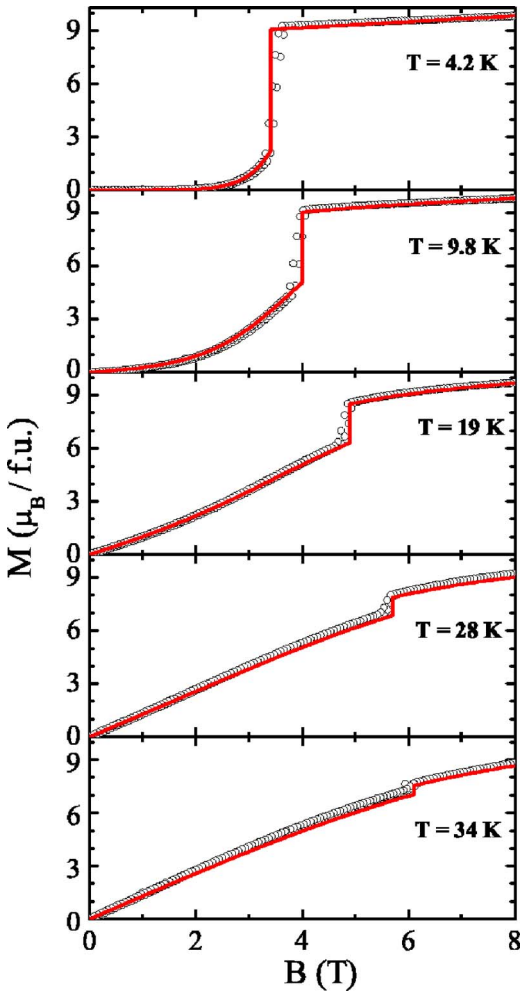

FIG. 6. (Color online) Experimental (symbols) and calculated (lines) magnetization curves of $TbFe_3(BO_3)_4$ for various temperatures with $B \| c$.

the calculated phase transition critical field exceeds the experimentally observed value and a similar relation between experimental and calculated critical fields takes place for all temperatures. On the other hand, if one takes the exchange parameter in the collinear phase to be $\sim 1\%$ less than that in the flop phase, the energy of the collinear phase increases slightly, the critical field decreases, and its calculated value is in good agreement with the experimental one (see Fig. 6). The difference between the values of the exchange parameter λ for two phases could be explained by the presence of the magnetoelastic effects accompanying the field-induced phase transition. In support of this hypothesis, it is known[6] that, in $GdFe_3(BO_3)_4$, with the S ion Gd^{3+}, the field-induced phase transition in the low-temperature phase ($T < 10$ K) results in a magnetostriction jump of the order of 2×10^{-5}. In $TbFe_3(BO_3)_4$, the highly anisotropic terbium ion should give a much more essential contribution to the magnetostriction at the field-induced spin-flop transition than the S ion Gd^{3+}. Indeed, calculations of the multipole moments $Q_{nm} = \alpha_n \langle O_n^m \rangle$ of the Tb^{3+} ion in $TbFe_3(BO_3)_4$ (which provide information on the rare-earth contribution to the magnetostriction[20]) have shown that their changes at the

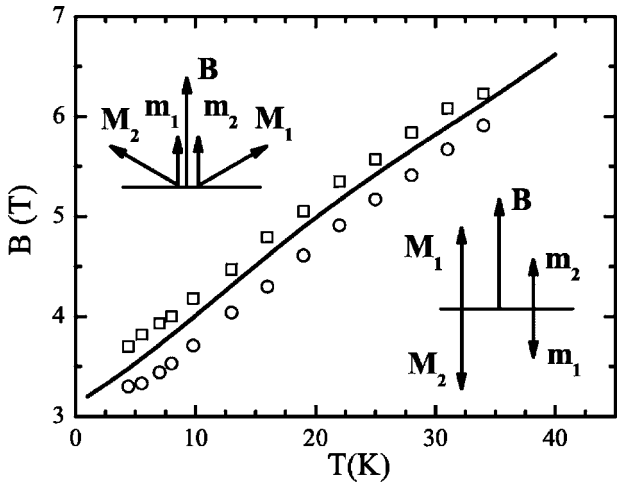

FIG. 7. The B-T phase diagram for the spin-flop transition in $TbFe_3(BO_3)_4$ at $B \| c$ [see Fig. 5(b)]. The symbols and the line represent the experimental data and the calculated phase boundary, respectively; the difference in experimental phase boundaries reflects a finite slope of $M(B)$ curve caused by a sample shape and hysteresis phenomena.

spin-flop phase transition are very significant.

To analyze the temperature evolution of the magnetization, we have to take into account the exchange between the Fe chains which is responsible for the three-dimensional ordering. This value of λ enters the Brillouin function in Eq. (7), the well-known explicit form of which is not given for the sake of brevity. It was chosen from the best agreement between experimental and calculated magnetization curves for all temperatures as $\lambda_2 = -2T/\mu_B$. The B-T phase diagram for the spin-flop transition (see Fig. 7) demonstrates good agreement between the calculated and experimental data. We emphasize that quantitative description of the magnetization isotherms of $TbFe_3(BO_3)_4$ in the mean-field approximation requires an introduction of two exchange parameters characterizing Fe-Fe antiferromagnetic interaction, λ_1 and λ_2. The λ_1 enters Eq. (8) for the energy and determines the critical field of the spin-flop transition B_c and the transverse susceptibility of the iron subsystem in the flop phase. The λ_2 determines the magnitude of iron magnetic moments M_i for specific temperature and field as well as the Néel temperature. The necessity of introducing two exchange parameters is a consequence of the chain structure of the ferroborate when considered in the mean-field approximation. The *intra*chain exchange interactions are described by λ_1, whereas the *inter*chain exchange interactions (which are responsible for the three-dimensional magnetic order) are described by λ_2. Our experimental data and the results of our theoretical analysis indicate that these two quantities are of the same order of magnitude.

B. ac magnetic susceptibility

As has already been discussed above, the strong anisotropy of the magnetic susceptibility is caused by the contribution of the Tb^{3+} ion with its Ising character of magnetic behavior. The $\chi(T)$ dependencies have been calculated using

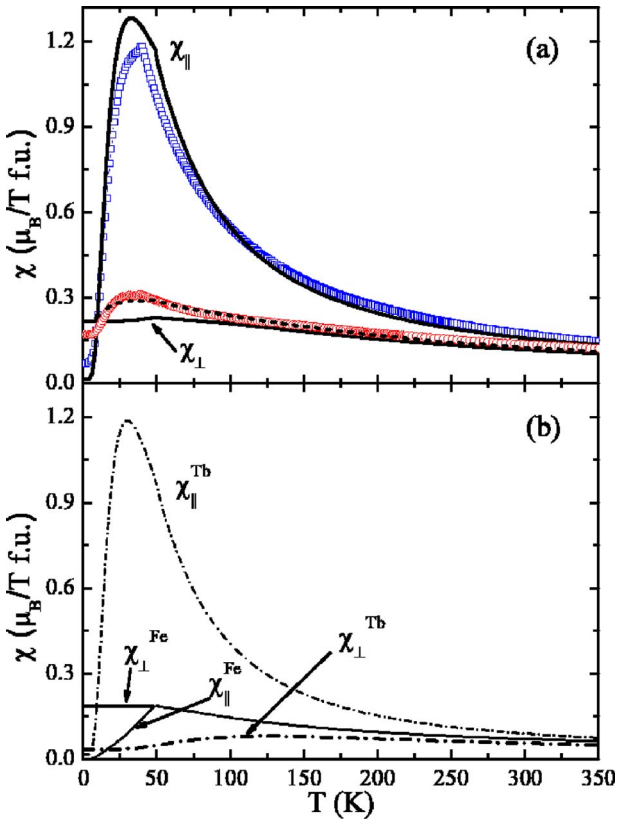

FIG. 8. (Color online) Temperature dependencies of the initial magnetic susceptibility in $TbFe_3(BO_3)_4$ along ($\chi_\parallel$) and perpendicular ($\chi_\perp$) to the trigonal axis. (a) Symbols are experimental points; solid thick lines are calculated curves for $\chi_\parallel$ and $\chi_\perp$; thick dashed line represents calculation of $\chi_\perp$ for the misorientation angle with regard to the basal plane in 3°. (b) Thin solid and dot-dashed lines are calculated curves for iron and terbium subsystems, respectively.

parameters of $TbFe_3(BO_3)_4$ derived from the analysis of the magnetization isotherms. However, as one can see in Fig. 8 the experimentally obtained and calculated $\chi_\perp(T)$ curves differ substantially. The nonzero susceptibility $\chi_\parallel$ at very low temperatures and a growth of $\chi_\perp$ upon increasing the temperature up to T_N could be ascribed to a misorientation of the sample by a few degrees with respect to the crystallographic axis. In fact, the inclusion of a misorientation by 3° with respect to the basal plane leads to a significantly better agreement between the calculated and experimental data. The variation of the crystal-field parameters within reasonable limits does not result in any significant changes in the description of the $\chi(T)$ dependencies; the agreement between experimental and calculated curves remains roughly the same.

A distinctive convexity of the experimental $\chi_\parallel(T)$ curve in the temperature range 30–35 K is associated with a Schottky-type anomaly, i.e., with the change of occupation of two low-lying terbium singlets. This anomaly can also be observed in the calculated curves, especially in the susceptibility of the Tb subsystem. The calculated Néel temperature is higher than the corresponding experimental value but this is a usual feature of the mean-field theory.

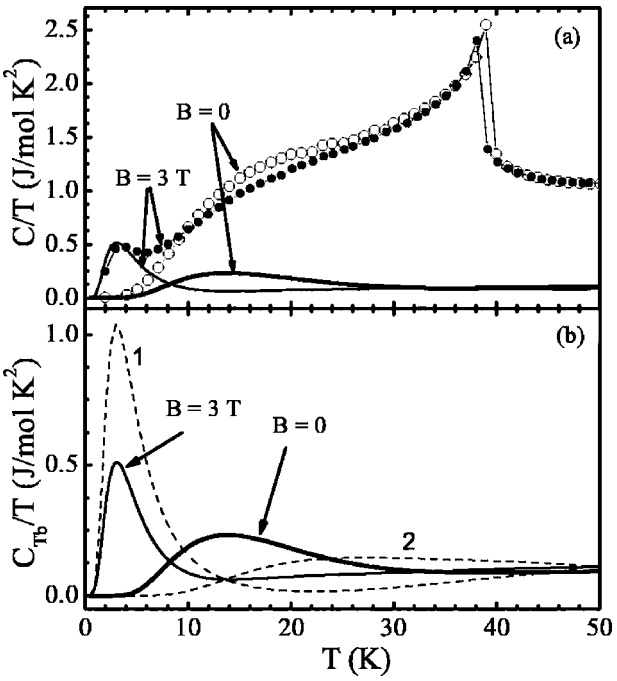

FIG. 9. (a) Specific heat of $TbFe_3(BO_3)_4$: open and closed symbols represent experimental data at $B=0$ and 3 T, respectively. Thick and thin solid lines correspond to calculations of the Tb contributions for $B=0$ and 3 T, respectively. (b) Calculated specific heat of the Tb subsystem: dashed lines 1 and 2 show calculated contributions for different sublattices at $B=3$ T.

C. Heat capacity

In the following, the specific heat and the effect of the magnetic field will be analyzed in terms of our approximation. The experimental specific-heat data in magnetic fields $B=0$ and 3 T along the c axis are presented in C/T vs T coordinates in Fig. 9(a). As one can see, the magnetic field shifts the Schottky anomaly to lower temperatures, specifically for $C(T)$ from ~20 K at $B=0$ to ~5 K at $B=3$ T. The anomaly at around 5 K is particularly evident since in this temperature range both the phonon and magnetic contributions are small.

The calculated temperature dependencies of the Tb contribution to the specific heat are presented in Fig. 9(b). The calculated $C_{Tb}(T)$ for $B=0$ demonstrates the Schottky anomaly around 20 K. As has already been mentioned above, the anomaly is caused by the occupation of the singlet level separated from the ground singlet by the temperature-dependent splitting due to the Tb-Fe interaction (Fig. 10).

Our analysis in Fig. 9(b) suggests that the Tb contribution to the specific heat is different for the two Tb sublattices if an external magnetic field is applied along the c axis. For the terbium sublattice with magnetic moments opposed to the field direction, the Schottky anomaly shifts to lower temperatures. This is easy to understand because an increase of the magnetic field leads to a decrease of the energy gap between two singlets (see Fig. 10). It means that an external field demagnetizes this terbium sublattice. For the other terbium sublattice, however, the energy gap between the two singlets increases, the increased external field magnetizes the sublat-

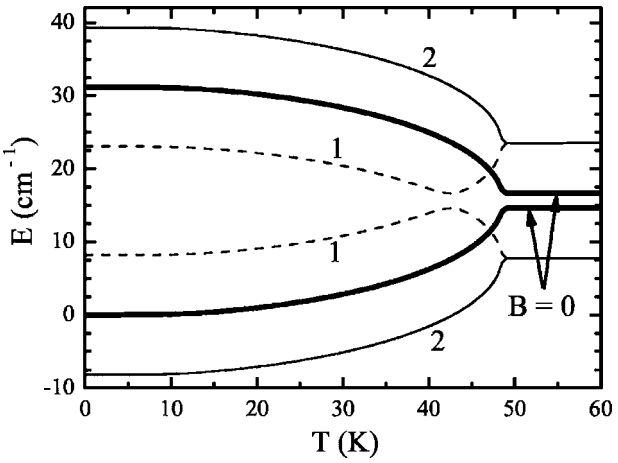

FIG. 10. Temperature dependencies of the splitting of the ground quasidoublet of the Tb^{3+} ion in $TbFe_3(BO_3)_4$ at $B=0$ and 3 T for sublattices with magnetic moments (1) opposite to the field direction and (2) along the field.

tice, and the Schottky anomaly moves to higher temperatures. We emphasize the agreement between the experimental and numerical data which confirms that the description of Tb-Fe coupling in $TbFe_3(BO_3)_4$ provided in this work is appropriate.

VI. CONCLUSIONS

Our measurements of the specific heat and the magnetization and the theoretical description of the experimental data provide a detailed understanding of the thermodynamical properties of $TbFe_3(BO_3)_4$. Our unified approach describes the presence of the spin-flop transition for magnetic fields applied parallel to the trigonal c axis and the related magnetization jump below T_N. Microscopically, the highly anisotropic magnetization data have been attributed to the Ising character of the Tb^{3+} ion in the trigonal crystal field. In addition, the presence of a Schottky anomaly in the specific-heat data around 20 K and its shift as a function of the applied magnetic field have been explained as the Tb contribution to specific heat in terms of two low-lying energy levels of the Tb^{3+} ions being split by f-d coupling.

In particular, our approximation considers the exchange interaction of the Fe subsystem as well as the coupling between Fe and Tb subsystems. The f-d coupling parameter has been determined and its value is in good agreement with available spectroscopic data. The antiferromagnetic exchange interaction in the iron subsystem has been described with the help of two parameters. The parameter λ_1 is responsible for bending the iron magnetic moments in the flop phase, which occurs against the intrachain exchange, and determines the spin-flop transition field; the parameter λ_2 is connected with the interchain exchange interaction responsible for the three-dimensional ordering, which controls the Néel temperature and magnitudes of the iron magnetic moments for specific temperatures and fields. The relation $|\lambda_1| > |\lambda_2|$ is naturally fulfilled because the Fe-O-Fe exchange paths within the chains are much shorter than the interchain exchange paths. The appearance of two exchange parameters is a special feature of consideration of magnetic properties of the compound with chain structure in the framework of the mean-field approximation, which is known to be of limited validity for description of magnetic lattices of lowered dimensionality. A substantial influence of the magnetoelastic effects which accompany the field-induced phase transition on the value of the molecular parameter responsible for bending the iron magnetic moments in the flop phase has been found.

ACKNOWLEDGMENTS

This work was partially supported by the Deutsche Forschungsgemeinschaft through 436 RUS 113/864/0-1 and HE 3439/1 and RFBR Grants No. 06-02-16088 and No. 07-02-00350. A.A.D. acknowledges support through Russian Federation's President Grant No. MK-4393.2006.2.

*Electronic address: npk@tu-bryansk.ru
†Electronic address: n.tristan@ifw-dresden.de

[1] J. A. Campa, C. Cascales, E. Gutierres-Puebla, M. A. Monge, I. Rasines, and C. Ruiz-Valero, Chem. Mater. **9**, 237 (1997).
[2] Y. Hinatsu, Y. Doi, K. Ito, M. Wakeshima, and A. Alemi, J. Solid State Chem. **172**, 438 (2003).
[3] A. D. Balaev, L. N. Bezmaternykh, I. A. Gudim, V. L. Temerov, S. G. Ovchinnikov, and S. A. Kharlamova, J. Magn. Magn. Mater. **258-259**, 532 (2003).
[4] R. Z. Levitin, E. A. Popova, R. M. Chtsherbov, A. N. Vasiliev, M. N. Popova, E. P. Chukalina, S. A. Klimin, P. H. M. van Loosdrecht, D. Fausti, and L. N. Bezmaternykh, JETP Lett. **79**, 531 (2004).
[5] A. K. Zvezdin, A. M. Kadomtseva, S. S. Krotov, A. P. Pyatakov, Yu. F. Popov, and G. P. Vorob'ev, J. Magn. Magn. Mater. **300**, 224 (2006).
[6] A. K. Zvezdin, S. S. Krotov, A. M. Kadomtseva, G. P. Vorob'ev, Yu. F. Popov, A. P. Pyatakov, L. N. Bezmaternykh, and E. A. Popova, JETP Lett. **81**, 272 (2005).
[7] F. Yen, B. Lorenz, Y. Y. Sun, C. W. Chu, L. N. Bezmaternykh, and A. N. Vasiliev, Phys. Rev. B **73**, 054435 (2006).
[8] J.-C. Joubert, W. B. White, and R. Roy, J. Appl. Crystallogr. **1**, 318 (1968).
[9] S. A. Klimin, D. Fausti, A. Meetsma, L. N. Bezmaternykh, P. H. M. van Loosdrecht, and T. T. M. Palstra, Acta Crystallogr., Sect. B: Struct. Sci. **61**, 481 (2005).
[10] A. N. Vasiliev, E. A. Popova, I. A. Gudim, L. N. Bezmaternykh, and Z. Hiroi, J. Magn. Magn. Mater. **300**, 382 (2006).
[11] A. N. Vasiliev, E. A. Popova, L. N. Bezmaternykh, V. L. Temerov, and Z. Hiroi, JETP **102**, 262 (2006).
[12] A. I. Pankrats, G. A. Petrakovskii, L. N. Bezmaternykh, and O. A. Bayukov, JETP **99**, 766 (2004).

[13] L. N. Bezmaternykh, V. L. Temerov, I. A. Gudim, and N. A. Stolbovaya, Crystallogr. Rep. **50**, 97 (2005).
[14] R. Klingeler, B. Büchner, S-W. Cheong, and M. Hücker, Phys. Rev. B **72**, 104424 (2005).
[15] H. Krug, M. Doerr, D. Eckert, H. Eschrig, F. Fischer, P. Fulde, R. Groessinger, A. Handstein, F. Herlach, and D. Hinz, Physica B **294-295**, 605 (2001); D. Eckert, R. Groessinger, M. Doerr, F. Fischer, A. Handstein, D. Hinz, H. Siegel, P. Verges, and K.-H. Mueller, *ibid.* **294-295**, 705 (2001).
[16] A. H. Morrish, *The Physical Principles of Magnetism* (Wiley, New York, 1965).
[17] C. Cascales, C. Zaldo, U. Caldino, J. Garcia Sole, and Z. D. Luo, J. Phys.: Condens. Matter **13**, 8071 (2001).
[18] E. P. Chukalina, D. Yu. Kuritsin, M. N. Popova, L. N. Bezmaternykh, S. A. Kharlamova, and V. L. Temerov, Phys. Lett. A **322**, 239 (2003).
[19] M. N. Popova, E. P. Chukalina, T. N. Stanislavchuk, and L. N. Bezmaternykh, Bull. Acad. Sci. RF, Phys. Ser. **70**, N11 (2006).
[20] N. P. Kolmakova, R. Z. Levitin, V. N. Orlov, and N. F. Vedernikov, J. Magn. Magn. Mater. **87**, 218 (1990); N. P. Kolmakova and I. B. Krynetskii, *ibid.* **130**, 313 (1994).